

Should Anisotropic Emission or Reabsorption of Nanoparticle Luminesces Be Optimized for Increasing Luminescent Solar Concentrator Efficiency?

Panagiotis Moraitis, Dick K. G. de Boer, P. Tim Prins, Celso de Mello Donegá, Kristaan Neyts, and Wilfried G. J. H. M. van Sark*

For the optimization of solar-to-electricity conversion efficiency of luminescent solar concentrators (LSCs), luminophores are treated as isotropic emitters. As rod-shaped nanocrystals are being developed, their anisotropic emission properties may be beneficial for LSC efficiency, as it is expected that escape cone losses can be reduced by proper alignment of nanorods (NRs). Herein, theoretical considerations and Monte Carlo ray-tracing simulations are used to examine the effect of anisotropic emission of luminophores on LSC performance, using nonspherical nanoparticles. Three different nanoparticles are examined with different Stokes shift and with two different quantum yield (QY) values (QY = 1 and QY = 0.7). In the case of a rod-shaped emitter with emission intensity distribution $I(\theta) \propto \sin^2 \theta$ aligned perpendicular to the lightguide plane, escape cone losses can potentially be reduced to $\approx 9\%$, compared to 25.5% for isotropic emission. For more realistic anisotropic emitters, escape cone losses reduce to $\approx 19\%$. Nonetheless, it is found that the useful emission of isotropic quantum dots with low reabsorption is much larger than that of aligning anisotropic emitting NRs with high reabsorption. Hence, focus on reducing reabsorption loss yields larger improvements in LSC device efficiency than focus on aligned NRs.

The recovery of the oil market later in the 1980s, and the continuously reduced cost of conventional solar cells to far below $1 \$ W^{-1}$ today, have drawn attention away from LSC technology. However, markets that require energy-harvesting façades such as building-integrated PV (BIPV) elements^[2] in combination with the development of stable nanocrystal-based luminophores have led to new research activities in this field.^[3–5]

The basic LSC design consists of an inexpensive glass or plastic lightguide with luminescent particles (luminophores) dispersed in the material, or spin-coated on top as a thin film, see Figure 1. Sunlight penetrates the top surface and part of it is absorbed by the luminophores and re-emitted at longer wavelengths. Emission typically takes place isotropically, with photons having random propagation directions in the transparent matrix, while luminophores exist^[7] that show anisotropic emission, as we will discuss later. The fraction

of the light that is emitted within the so-called escape cone leaves the lightguide, whereas the rest is trapped by total internal reflection and travels toward the edges, where small PV cells can be attached and convert the energy of photons into useful electricity.

The most critical element of an LSC device is the selected luminophore as it is essential for the absorption of incoming photons and re-emission of the absorbed energy as red-shifted photons with a different direction compared to the incoming one, and thus fundamental for the solar concentration. The

1. Introduction

The luminescent solar concentrator (LSC) was introduced over four decades ago^[1] as a device that allows increased photon flux, which is the main advantage of reflective and refractive concentrating optical systems, but without requiring direct sunlight and active tracking mechanisms. It was developed as a cheap alternative to crystalline silicon photovoltaic (PV) cells, in a period where the oil crisis had increased the cost of energy drastically.

Dr. P. Moraitis, Prof. W. G. J. H. M. van Sark
Copernicus Institute of Sustainable Development
Utrecht University
Princetonlaan 8a, 3584 CB Utrecht, The Netherlands
E-mail: w.g.j.h.m.vansark@uu.nl

 The ORCID identification number(s) for the author(s) of this article can be found under <https://doi.org/10.1002/solr.202000279>.

© 2020 The Authors. Published by Wiley-VCH GmbH. This is an open access article under the terms of the Creative Commons Attribution License, which permits use, distribution and reproduction in any medium, provided the original work is properly cited.

DOI: 10.1002/solr.202000279

Dr. D. K. G. de Boer
Solumineus
Transvaalkade 134hs, 1091 LT Amsterdam, The Netherlands

P. T. Prins, Dr. C. de Mello Donegá
Debye Institute for Nanomaterials Science
Utrecht University
P.O. Box 80000, 3508 TA Utrecht, The Netherlands

Prof. K. Neyts
LCP Group
ELIS Department
Ghent University
Technologiepark 126, 9052 Gent, Belgium

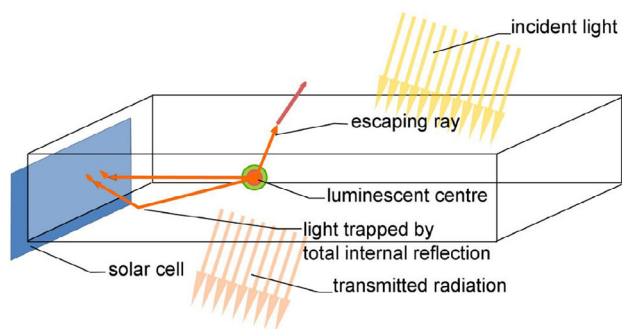


Figure 1. Schematic representation of an LSC device under illumination.^[6]

luminophore should exhibit a broad absorption spectrum with a high absorption coefficient to successfully absorb the incoming photons, a high photoluminescence quantum yield (QY) so that the captured photons will be re-emitted and a large Stokes shift (i.e., difference between emission and absorption maximum) that will ensure that the emitted photons will not be reabsorbed by other luminophores in the host material.^[8] So far in the development of LSC devices, and specifically in the selection of the appropriate luminophore, the attention was focussed mainly on how to improve these three parameters while taking for granted other types of losses, such as light reflection from the top surface, light scattering, and escaping of photons through the escape cone, which are inherent to this type of technology.

The latter is a very important loss, and for a luminophore that emits photons isotropically in a lightguide with refractive index of 1.5, the expected probability that the photon will be emitted within the escape cone is 25.46%.^[9] However, in a real-life scenario that includes a large number of luminophores in a lightguide and where reabsorption effects are very likely to take place, it is estimated that 40–55% of all the absorbed energy is lost in that way in a $5 \times 5 \text{ cm}^2$ device.^[10] The main strategies that have been developed so far to tackle the escape cone losses are 1) the use of aligned dichroic dyes in liquid crystals,^[11,12] 2) the application of wavelength-selective mirrors that allow incoming light to enter the lightguide and be absorbed, but are reflective for wavelengths emitted by the luminophore,^[9,10,13–15] and 3) the use of photonic crystal waveguides in which the luminophores are embedded.^[16] More recently, alignment of a pair of luminophores, i.e., a sphere-shaped energy donor and a rod-shaped emitter, both organic, has been reported to decrease escape cone losses by 10% relative.^[17]

In this article, we examine the effect of anisotropic emission of luminophores and their alignment on LSC performance. The anisotropy derives from the nonspherical shape of dot-in-rods, or nanorods (NRs), which typically consist of a spherical semiconductor nanocrystal core surrounded by a rod-like shell.^[18,19] Alignment of NRs has been experimentally demonstrated,^[20–24] e.g., NRs will automatically lie flat on a surface after solvent evaporation.^[21] Vertical alignment is also possible under a high electric field,^[25] but only in solution.^[22] The simulations presented here will provide insight into the expected impact of the experimental control over NR alignment on the efficiency of LSCs. We will compare \sin^2 , \cos^2 , and isotropic emitters, as well as a realistic NR emitter (see Figure 2). Considering

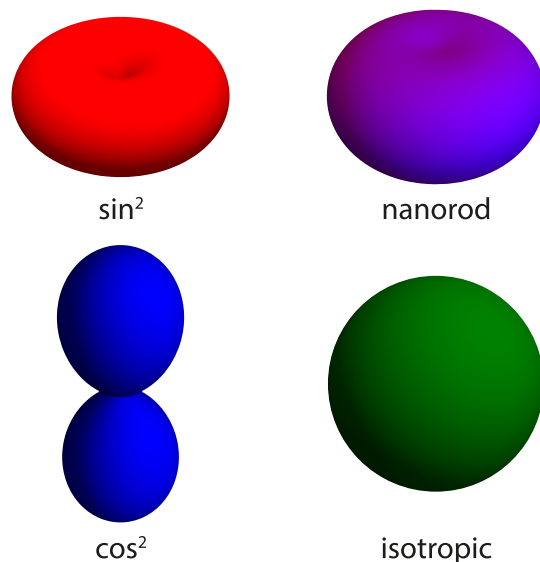


Figure 2. Emission pattern of \sin^2 (red), \cos^2 (blue), and isotropic (green) emitters, and a realistic NR emitter (purple).

depolarization effects and the quantum mechanical splitting of the energy levels, we will theoretically derive anisotropy effects on emission patterns. We will then use that to define the emission behavior of rod-shaped emitters in a Monte Carlo ray-trace simulation model for a $10 \times 10 \times 0.5 \text{ cm}^3$ LSC plate. Escape cone loss and edge emission of the LSC plate will be evaluated based on emitter type, reabsorption coefficient, and QY losses.

2. Results and Discussion

2.1. Escape Fraction for Anisotropic Emission Patterns—Theory

For a photon emitter in a lightguide with intensity distribution $I(\theta)$, assuming no azimuthal dependence, the escape fraction F_{esc} from the large sides of the plate is expressed as

$$F_{\text{esc}} = \frac{\int_0^{\theta_c} I(\theta) \sin(\theta) d\theta}{\int_0^{\pi/2} I(\theta) \sin(\theta) d\theta} \quad (1)$$

in which θ_c is the critical angle for total reflection in the lightguide material.^[9,10] For an ordinary isotropic (spherical) emitter, $I(\theta)$ is constant, so that Equation (1) simplifies to

$$F_{\text{esc,iso}} = 1 - \cos \theta_c \quad (2)$$

which amounts to 0.2546 if the refractive index of the plate $n = 1.5$. The critical angle θ_c can also be expressed as function of n

$$\theta_c = \sin^{-1} \left(\frac{1}{n} \right) \quad (3)$$

and equals $\theta_c = 41.8^\circ$ for $n = 1.5$.

Let us now define the angle between the long axis of a nonspherical NR and the plate surface normal as Ω . For this

rod-shaped emitter with the dipole transition parallel to the long axis (see Figure 1a in the Supporting Information), the intensity distribution is $I(\theta) \propto \sin^2 \theta$ in case the rod is aligned perpendicular to the plate ($\Omega = 0^\circ$). We then derive

$$F_{\text{esc},\sin}^0 = 1 + (\cos 3\theta_c - 9 \cos \theta_c)/8 \quad (4)$$

which amounts to 0.089 for $n = 1.5$. Hence, compared to the isotropic emitter case, the escape fraction is greatly reduced by nearly a factor of 3 for emitters with \sin^2 intensity pattern. If the rod is aligned parallel to the plate ($\Omega = 90^\circ$) (Figure 1b in the Supporting Information), the escape fraction is

$$F_{\text{esc},\sin}^{90} = 1 - (\cos 3\theta_c + 15 \cos \theta_c)/16 \quad (5)$$

For $n = 1.5$, this amounts to $F_{\text{esc},\sin}^{90} = 0.338$, which is $\approx 50\%$ larger than in the isotropic emitter case.

For rod angles Ω between these extremes, one can write

$$F_{\text{esc},\sin}^\Omega = F_{\text{esc},\sin}^0 \cos^2 \Omega + F_{\text{esc},\sin}^{90} \sin^2 \Omega \quad (6)$$

Figure 3 shows the escape fraction as a function of Ω for this case (red line), and it is compared with that of an isotropic emitter of which the escape fraction clearly is constant (green line).

Another extreme is that of a dipole transition perpendicular to the long axis in case the rod is aligned perpendicular to the plate, which is represented by \cos^2 emission. The behavior as a function of Ω in this case is shown in Figure 3 (blue line). The equations used for the graph can be found in the Supporting Information. We note that our theoretical results are in good correspondence to theoretical and experimental results on anisotropic emission for alignment of dichroic dyes as reported by Verbunt et al.^[12]

In reality, the behavior of a NR emitter will be a combination of a \sin^2 and a \cos^2 emitter, resulting in an emission pattern between that of an isotropic and a \sin^2 emitter. There are two physical effects that contribute to this. The first effect is

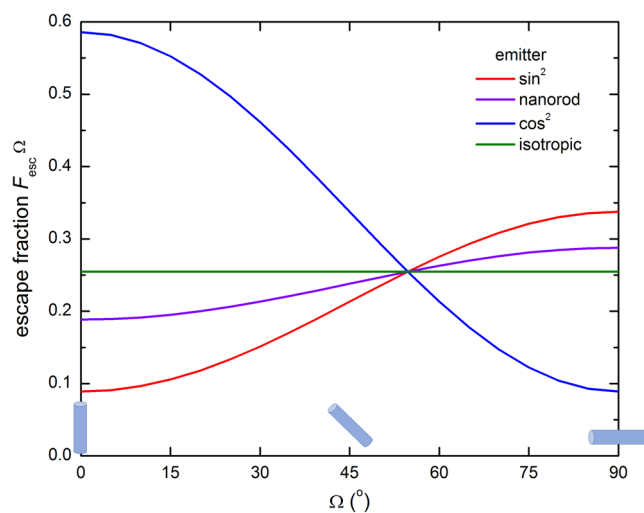


Figure 3. Escape fraction of a rod-shaped emitter with rod angle varying from perpendicular to parallel with respect to the lightguide plane. Green: isotropic emitter, red: $I(\theta) \propto \sin^2 \theta$, blue: $I(\theta) \propto \cos^2 \theta$, purple: NR emitter (combination of isotropic and \sin^2 emitter).

depolarization by the medium surrounding the emitting species.^[26,27] Because of the elongated shape of a rod, the depolarization of an electric field in the rod will be different for directions parallel and perpendicular to the long axis. The emission intensities are proportional to the squares of the so-called local-field fractions f_{\parallel} and f_{\perp} . The second physical effect is the quantum mechanical splitting between energy levels from which emission parallel and perpendicular to the long axis can occur.^[28] The parallel case corresponds to a 1D dipole, with relative intensity p_1 , and the perpendicular case to a 2D degenerate dipole, with relative intensity p_2 . Combining the two physical effects, we have

$$I(\theta) \propto q_1 \sin^2 \theta + q_2 (\cos^2 \theta + 1) \quad (7)$$

with $q_1 = p_1 f_{\parallel}^2$ and $q_2 = p_2 f_{\perp}^2$. The escape fractions can be derived as follows (see Supporting Information)

$$F_{\text{esc},\text{NR}}^0 = \frac{F_{\text{esc},\text{iso}}^0 + \frac{1}{3} \left(\frac{q_1}{q_2} - 1 \right) F_{\text{esc},\text{sin}}^0}{1 + \frac{1}{3} \left(\frac{q_1}{q_2} - 1 \right)} \quad (8)$$

$$F_{\text{esc},\text{NR}}^{90} = \frac{F_{\text{esc},\text{iso}}^{90} + \frac{1}{3} \left(\frac{q_1}{q_2} - 1 \right) F_{\text{esc},\text{sin}}^{90}}{1 + \frac{1}{3} \left(\frac{q_1}{q_2} - 1 \right)} \quad (9)$$

For $q_1/q_2 = 1, \infty, -1$, or 3 , these equations represent an isotropic, \sin^2 , \cos^2 , or actual NR emitter, respectively. The value $q_1/q_2 = 3$ is typical for what has been experimentally determined for CdSe/CdS dot core/rod shell NRs (see Supporting Information). It reflects contributions to $I(\theta)$ of an isotropic and a \sin^2 emitter, and we find $F_{\text{esc},\text{NR}}^0 = 0.188$ and $F_{\text{esc},\text{NR}}^{90} = 0.288$ for $n = 1.5$. Compared to the isotropic emitter case, the escape fraction for rods aligned perpendicular to the plate is lower, but it is higher than for the \sin^2 emitter case. For rods aligned parallel to the plane this is reversed, but with lower relative difference. Figure 3 (purple line) shows the behavior for $q_1/q_2 = 3$ as a function of Ω . It can be seen that the escape fraction for vertical rods is larger than for pure \sin^2 emitters and smaller than for the isotropic case up to $\Omega \approx 55^\circ$.

2.2. Simulation Results

The absorption cross-sections (per nanocrystal) and normalized emission spectra of the three different types of nanocrystals, i.e., core-only CdSe quantum dots (QDs)^[29] with large reabsorption, CdSe/CdS dot core/rod shell NRs^[30] with small reabsorption, and Mn^{2+} -doped ZnSe QDs^[31] with no reabsorption, are shown in Figure 4. Absorption cross-sections per nanocrystal vary over two orders of magnitude, with the CdSe/CdS dot core/rod shell NRs having the highest cross-section, due to their largest volume. The concentration of the nanocrystals is adjusted such that the transmission of the solar spectrum (AM1.5 G, 300–650 nm) of the 0.5 cm thick LSC plates is 95%. A high transmission was necessary for the simulations, as for lower transmission values most of the waveguided light in the CdSe core-only nanocrystals based LSC is lost due to the high reabsorption coefficient. Details are given in Table 1. We further denote these nanocrystals with terms “high”, “low”, and “none” reflecting the amount of reabsorption (indicated in Table 1, last line). Absorption coefficients

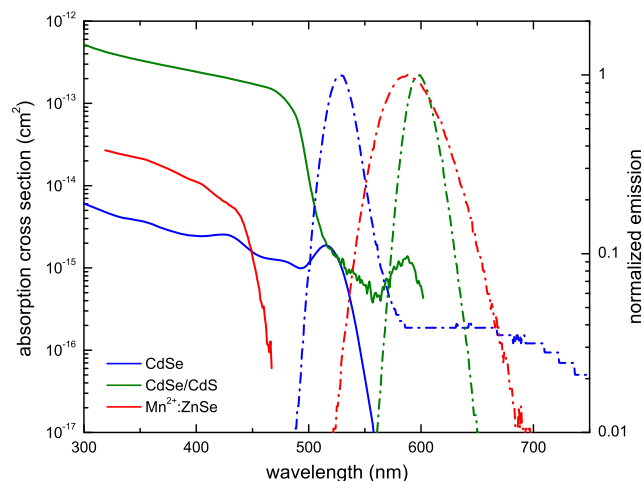


Figure 4. Absorption cross-section per nanoparticle (solid lines) and normalized emission spectra (dash-dot lines) of core-only CdSe QDs, CdSe/CdS dot core/rod shell NRs, and Mn²⁺:ZnSe QDs.

Table 1. Properties of nanocrystals.

	CdSe	CdSe/CdS	Mn ²⁺ :ZnSe
Absorption peak [nm eV ⁻¹]	516/2.40	487/2.55	437/2.84
Emission peak [nm eV ⁻¹]	528/2.35	599/2.07	590/2.10
Absorption cross section at 300 nm (10 ⁻¹⁴ cm ²) ^{a)}	0.61	52	3.3
Concentration [10 ⁻¹² mol cm ⁻³]	170	2.0	62
Reabsorption coefficient A _{ra} [10 ⁻³ cm ⁻¹]	84/high	0.65/low	0/none

^{a)}The absorption cross-section is calculated for luminophores in a medium with refractive index 1.5 (PMMA) using ref. [26].

of the simulated LSCs can be found in the Supporting Information. The emission anisotropy of the nanocrystal is determined by the q_1/q_2 value as described earlier, and we further discern nanocrystals on the level of reabsorption.

In our simulations, we assume that every luminophore can be either an isotropic emitter or an anisotropic emitter (with three different values for q_1/q_2). In this way, we are going to examine whether optimal alignment of nanocrystals, given their three types and QY, will potentially lead to higher LSC device efficiencies compared with nanocrystals with isotropic emission.

We use two different QY values. For QY = 1, every absorbed photon is re-emitted. This is currently a nonrealistic scenario as most QDs (and NRs) exhibit lower QY values, but our purpose here is to examine the limit of QD-based LSC technology. We note that CdSe/CdS core/shell QDs with QY as high as 0.996 have been recently reported, showing that the QYs of QDs and other semiconductor nanocrystals are not fundamentally limited and may reach near-unity values.^[32] A more realistic value of QY is 0.7 is also used, which most high-quality QDs can reach either in liquid solution or in thin film.

Reabsorption or self-absorption will occur when there is a finite probability for a luminophore to absorb the light emitted

by the same species. A reabsorption coefficient can be quantified by calculating the overlap between absorption and emission spectrum as follows: $A_{ra} = \int A(\lambda)E(\lambda)d\lambda / \int E(\lambda)d\lambda$, with $A(\lambda)$ the absorption coefficient of the simulated LSC and $E(\lambda)$ the emission spectrum of the luminophore. It thus provides a measure of the emission that is absorbed by luminophores while the emitted light travels through the lightguide. We assume that reabsorption is independent of the polarization and the orientation of the NRs. We also note that by using this definition, the effect of consecutive reabsorption events may be over-estimated. Red photons have a smaller chance to be reabsorbed than green ones. However, in this article, the number of multiple reabsorption events is small as absorption in the LSC is low.

From the absorption and emission spectra of the three materials investigated (Figure 4), in particular the overlap of absorption and emission spectrum, it is clear that the reabsorption of emitted light in case of the core-only CdSe QDs is high: we calculate $A_{ra} = 84 \times 10^{-3} \text{ cm}^{-1}$. For both the CdSe/CdS dot core/rod shell, and the Mn²⁺:ZnSe QDs, A_{ra} is much smaller, i.e., $0.65 \times 10^{-3} \text{ cm}^{-1}$ and 0 cm^{-1} , respectively. Hence, the qualifications used for reabsorption: “high”, “low”, and “none” in Table 1. Note, in the aforementioned, we did not consider polarization effects, nor anisotropy of absorption. This implies that the angular emission probability is assumed to be the same after reabsorption as for direct absorption of sunlight. This is not necessarily true, as light emitted by vertical rods is polarized in such a way that it is more easily absorbed by vertical rods. So, for vertical rods (rod rotation $\Omega = 0^\circ$), the effect of reabsorption may be somewhat larger than simulated.

Figure 5 shows the behavior of the three types of luminophores for several values of q_1/q_2 as a function of the rod rotation angle Ω . It is assumed that all quantum rods dispersed in the LSC plate have the same angle Ω . In Figure 5, the effect of different q_1/q_2 values on the escape cone fraction (top panels) and the edge emission fraction (bottom panels) are shown, both for QY = 1 (closed symbols, solid line) and QY = 0.7 (open symbols, dashed line). The edge emission is defined as the amount of photons that is successfully guided to all four edges of the LSC device, which could potentially be absorbed in the solar cell(s) mounted at the edges. Moreover, we take into consideration only the fraction of photons that has been absorbed by the LSC.

It is clear that edge and escape fractions of low and no reabsorption nanoparticles are similar, while those of the high reabsorption nanoparticle are higher. For the nanoparticles with low and no reabsorption, the results are in excellent agreement with the theoretical results, as shown in Figure 3. These curves are also shown in Figure 5, for QY = 1 (solid line) and QY = 0.7 (dashed line). We note that as 5% of the photons are absorbed and $\approx 90\%$ of them reach the sides, only 45 000 photon rays are effectively used, resulting in an expected error (1 sigma) of $\approx 0.5\%$. So, the observed difference of 0.7% (91.8% [simulation] versus 91.1% [theory]) is within that range. Also, the differences in the results for low and no reabsorption are small. This is due to the size of the LSC. The differences would be larger for large-sized LSCs.

We find that the highest edge emission fraction is 91.8% for no reabsorption nanoparticles for $q_1/q_2 = \infty$ (sin² emitter) and

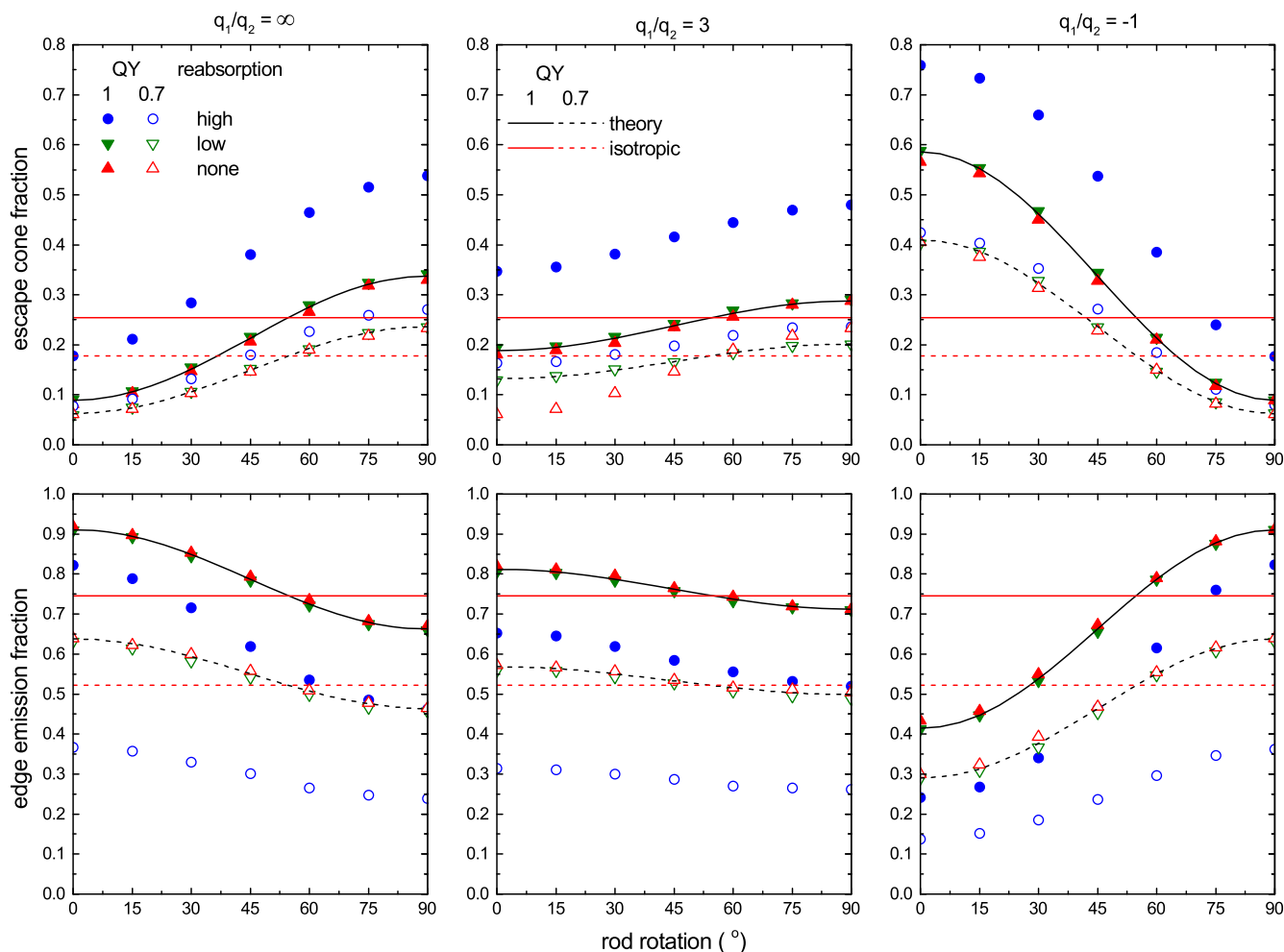


Figure 5. Escape cone fraction (top panels) and edge emission fraction (bottom panels) as a function of rod rotation angle Ω for QY = 1 (solid symbols and lines) and QY = 0.7 (open symbols and dashed lines). $q_1/q_2 = \infty$ (left panels, \sin^2 emitter), $q_1/q_2 = 3$ (middle panels, NR emitter), $q_1/q_2 = -1$ (right panels, \cos^2 emitter). Lines are from theory (Figure 3), and the isotropic values (red, $q_1/q_2 = 1$).

when the nanoparticles are aligned perpendicular to the LSC plane ($\Omega = 0^\circ$). For $q_1/q_2 = 3$ (realistic NR emitter), there is a small reduction and the maximum edge emission drops to 82.0%, again for no reabsorption nanoparticles with the same alignment. For $q_1/q_2 = -1$ (\cos^2 emitter), the cosine factor in Equation (7) becomes prominent, which changes the emission pattern and the maximum concentration to the edges (91.1%) is achieved when the NRs are aligned parallel to the LSC plane ($\Omega = 90^\circ$). The fact that the escape cone losses are higher for QY = 1 than QY = 0.7 might seem counter intuitive, but in the latter case, a number of photons is lost as they are never re-emitted. It is also important to highlight that the effects of reabsorption differ with varying alignment, QY value and emission anisotropy. In case of high levels of reabsorption, we observe that the edge emission can be reduced down to 82.2% (QY = 1) and 36.7% (QY = 0.7) for $q_1/q_2 = \infty$ (\sin^2 emitter) with a concomitant increase in escape cone loss. For the other lumino-phores, with low and no reabsorption, the edge emission is reduced from 91.8% for QY = 1 to 63.9% for QY = 0.7, which is in excellent agreement with theory. In summary, from

Figure 5, it is clear that for certain type of emitters, edge emission is larger (and escape cone losses are lower) than in case of isotropic emission and that reabsorption and QY losses are critical for the overall performance of an LSC device regardless of the orientation of the NR.

In **Figure 6**, the edge emission fraction of all the absorbed photons for rod rotation $\Omega = 0^\circ$ is presented for various levels of reabsorption. For the scenario where QY = 1 and \sin^2 emission (Figure 6a), the edge emission can reach 92% for the vertically aligned rods when there is no or low reabsorption. The effect of reabsorption is seen to be smaller in the case of vertically aligned rods (change from 91.8% to 82.2%, for the high reabsorption nanoparticle) than in the case of isotropic emission (change from 75.1% to 56.2%). The $q_1/q_2 = 3$ case, which represents an emission pattern closer to realistic NRs, exhibits lower values for the aligned NRs compared to a \sin^2 emitter, i.e., 82.0% for no reabsorption to 65.3% for high reabsorption.

The QY = 0.7 case (Figure 6b), with \sin^2 emission, exhibits edge emission values reduced by approximately 30% for the case without reabsorption (from 91.8% to 63.9%) and by about 55%

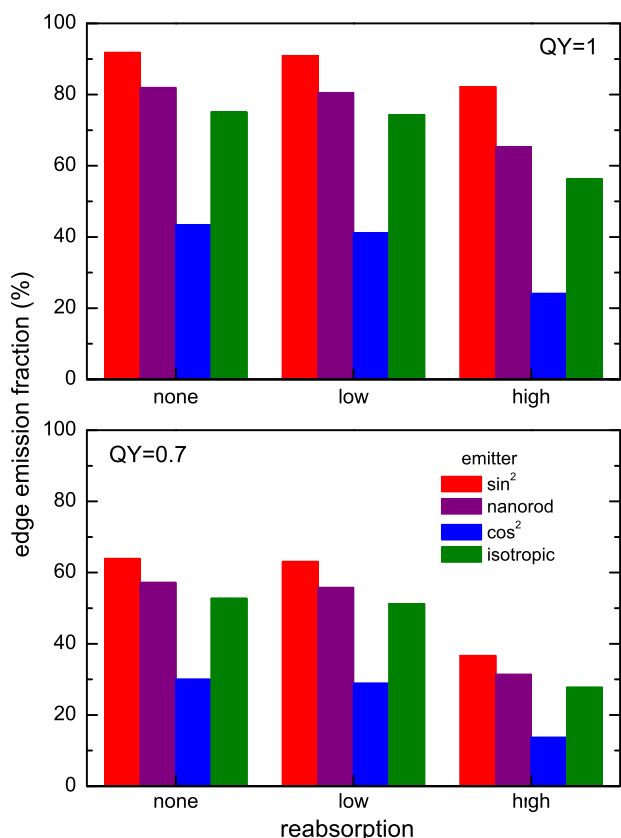


Figure 6. Edge emission fraction for a) $QY = 1$ and b) $QY = 0.7$, for all luminophores aligned vertically ($\Omega = 0^\circ$) and for all emitter types: \sin^2 ($q_1/q_2 = \infty$), NR ($q_1/q_2 = 3$), \cos^2 ($q_1/q_2 = -1$), and isotropic ($q_1/q_2 = 1$).

(from 82.2% to 36.7%) for the case with high reabsorption. For isotropic emission, the edge emission reduces to 52.8% for no reabsorption and 27.8% for high reabsorption. For $q_1/q_2 = 3$, edge emission values are reduced to 57.2% for no reabsorption to 31.4% for high reabsorption, which is a similar relative reduction compared with a \sin^2 emitter.

It is now interesting to compare two realistic cases, i.e., a QD isotropic emitter ($q_1/q_2 = 1$) with high reabsorption and a NR anisotropic emitter ($q_1/q_2 = 3$) with no reabsorption, both with $QY = 0.7$. Edge emissions are 27.8% and 57.2%, respectively. However, considering a QD isotropic emitter without reabsorption shows edge emission of 52.8%, very close to the value for the NR emitter. Another case is based on actual reported QY yield values approaching 1.^[8] A QD isotropic emitter with high reabsorption shows edge emission of 56.2%, hence about equal to a zero-reabsorption NR emitter with $QY = 0.7$. Reducing the reabsorption to zero leads to edge emission of 75.1% for the QD isotropic emitter. If one compares the effect of alignment of NRs to isotropic emitters on edge emission, Figure 6 clearly evidences that at similar QY and reabsorption, alignment increases edge emission by 4% to 10%-point, while decreasing reabsorption loss from high to low or zero has a much larger effect, and ranges from 25% to 30%-point. It is thus more sensible to focus

experimental efforts on reducing reabsorption rather than on achieving alignment of NRs.

3. Conclusion

In conclusion, in this research, the effects of reabsorption, QY, and emission anisotropy were investigated for different nanocrystals for use in LSC devices. It was shown that all have a significant but differing effect on the edge emission fraction, and thus overall performance of an LSC device. In case of a \sin^2 emitter, more than 90% of all the absorbed photons could reach the sides of the device with a low or zero reabsorption emitter. That would set new standards for the LSC technology as the device efficiency in this case would be limited mainly by the absorption capacity of the luminophore. In case of a realistic NR emitter that combines \sin^2 and isotropic emission, the optical efficiency can still reach impressive values with 82.2% of absorbed photons reaching the side of the device with $QY = 1$ and no reabsorption. Both values are higher than for isotropic QD emissions, which shows edge emission of 75.1% of absorbed photons. Lowering QY from 1 to 0.7 changes the edge emission significantly, but only decreases the differences between different cases. Most importantly, the results show that reducing reabsorption loss yields larger improvement in edge emissions compared to changing the emission from isotropic to anisotropic, i.e., from using spherical QDs to aligned NRs. For $QY = 1$ (0.7), the edge emission is 75.1% (52.8%) for isotropic QDs with low reabsorption versus 65.3% (31.4%) for NRs with high reabsorption. Moreover, as the alignment of NRs is experimentally challenging,^[20–25] while yielding limited benefits, we conclude that as a design rule it is better to focus on limiting reabsorption to increase LSC device efficiency.

4. Experimental Section

We used the PVtrace^[33] model for Monte Carlo ray tracing simulations. In the case of a spherical QD, photon emission takes place isotropically, meaning that the emitted photon can have any direction, and the emitted light is uniformly distributed. Hence, the probability distribution function (PDF) of the emission as function of the solid angle ω is constant: $p(\omega) = c$. For the simulation of the emission of a rod-shaped emitter using randomly generated numbers, the PDF is not constant ($p(\omega) \neq c$). In the Supporting Information, we describe a nonconstant PDF in spherical coordinates and show how anisotropic emission can be implemented in Monte Carlo simulations. We have modified the emission routine of PVtrace to allow for nonisotropic emission.

Simulations were performed using 1 million photons for a $10 \times 10 \times 0.5 \text{ cm}^3$ LSC plate of polymethylmethacrylate (PMMA) with $n = 1.5$ using three different nanocrystal types as luminophores. As proxy for the three different types of nanocrystals, we selected core-only CdSe QDs^[29] with large reabsorption, CdSe/CdS dot core/rod shell NRs^[30] with small reabsorption, and Mn^{2+} -doped ZnSe QDs^[31] with no reabsorption. These types of nanocrystals thus differ in absorption and emission spectrum, QY, Stokes shift, and emission anisotropy, as these are crucial parameters for LSC device efficiency.^[34]

Supporting Information

Supporting Information is available from the Wiley Online Library or from the author.

Acknowledgements

Financial support is gratefully acknowledged from Climate-KIC via the project Console, from TKI-Urban Energy via the project Trapeze, and from the Dutch Research Council (NWO) and Flanders Innovation & Entrepreneurship (VLAIO) via the project Q-Lumicon. The authors thank participants in these projects for valuable discussions at various stages of the research.

Conflict of Interest

The authors declare no conflict of interest.

Keywords

anisotropy, luminescent solar concentrators, nanocrystals, nanorods

Received: June 4, 2020

Revised: July 27, 2020

Published online: August 16, 2020

-
- [1] A. Goetzberger, W. Greubel, *Appl. Phys.* **1977**, *14*, 123.
 [2] W. van Sark, *Renew. Energy* **2013**, *49*, 207.
 [3] F. Meinardi, F. Bruni, S. Brovelli, *Nat. Rev. Mater.* **2017**, *12*, 17072.
 [4] M. R. Bergren, N. S. Makarov, K. Ramasamy, A. Jackon, R. Guglielmetti, H. McDaniel, *ACS Energy Lett.* **2018**, *3*, 520.
 [5] L. M. Wheeler, V. M. Wheeler, *ACS Energy Lett.* **2019**, *4*, 2130.
 [6] Z. Krumer, S. Pera, R. Van Dijk-Moes, Y. Zhao, A. De Brouwer, E. Groeneveld, W. Van Sark, R. Schropp, C. De Mello Donegá, *Sol. Energy Mater. Sol. Cells* **2013**, *111*, 57.
 [7] P. P. C. Verbunt, C. Sánchez-Somolinos, D. J. Broer, M. G. Debije, *Opt. Express* **2013**, *21*, A485.
 [8] F. Meinardi, A. Colombo, K. A. Velizhanin, R. Simonutti, M. Lorenzon, L. Beverina, R. Viswanatha, V. I. Klimov, S. Brovelli, *Nat. Photon.* **2014**, *8*, 392.
 [9] W. Van Sark, K. Barnham, L. Slooff, A. Chatten, A. Büchtemann, A. Meyer, S. McCormack, R. Koole, D. Farrell, R. Bose, E. Bende, A. Burgers, T. Budel, J. Quilitz, M. Kennedy, T. Meyer, C. De Mello Donegá, A. Meijerink, D. Vanmaekelbergh, *Opt. Express* **2008**, *16*, 26.
 [10] M. G. Debije, P. P. C. Verbunt, *Adv. Energy Mater.* **2011**, *2*, 12.
 [11] P. P. C. Verbunt, A. Kaiser, K. Hermans, C. W. M. Bastiaansen, D. J. Broer, M. G. Debije, *Adv. Funct. Mater.* **2009**, *19*, 2714.
 [12] P. P. C. Verbunt, T. M. de Jong, D. K. G. de Boer, D. J. Broer, M. G. Debije, *Eur. J. Phys. Appl. Phys.* **2014**, *67*, 10201.
 [13] M. G. Debije, M.-P. Van, P. P. C. Verbunt, M. J. Kastelij, R. H. L. Van der Blom, D. J. Broer, C. W. M. Bastiaansen, *Appl. Opt.* **2010**, *49*, 745.
 [14] T. Markvart, *J. Appl. Phys.* **2006**, *99*, 26101.
 [15] J. C. Goldschmidt, M. Peters, A. Bösch, H. Helmers, F. Dimroth, S. W. Glunz, G. Willeke, *Sol. Energy Mater. Sol. Cells* **2009**, *93*, 176.
 [16] H. C. Bauser, C. R. Bukowsky, M. Phelan, W. Weigand, D. R. Needell, Z. C. Holman, H. A. Atwater, *ACS Photon.* **2020**, <https://dx.doi.org/10.1021/acsp Photonics.0c00593>.
 [17] B. Zhang, C. Gao, H. Soleimaninejad, J. M. White, T. A. Smith, D. J. Jones, K. P. Ghiggino, W. W. H. Wong, *Chem. Mater.* **2019**, *31*, 3001.
 [18] C. de Mello Donega, *Chem. Soc. Rev.* **2011**, *40*, 1512.
 [19] S. Vezzoli, M. Manceau, G. Leménager, Q. Glorieux, E. Giacobino, L. Carbone, M. D. Vittorio, A. Bramati, *ACS Nano* **2015**, *9*, 7992.
 [20] M. Zanella, R. Gomes, M. Povia, C. Giannini, Y. Zhang, A. Riskin, M. Van Bael, Z. Hens, L. Manna, *Adv. Mater.* **2011**, *23*, 2205.
 [21] F. Pietra, F. T. Rabouw, W. H. Evers, D. V. Byelov, A. V. Petukhov, C. de Mello Donegá, D. Vanmaekelbergh, *Nano Lett.* **2012**, *12*, 5515.
 [22] J. S. Kamal, R. Gomes, Z. Hens, M. Karvar, K. Neyts, S. Compernelle, F. Vanhaecke, *Phys. Rev. B* **2012**, *85*, 035126.
 [23] P. D. Cunningham, J. B. Souza, I. Fedin, C. She, B. Lee, D. V. Talapin, *ACS Nano* **2016**, *10*, 5769.
 [24] S. K. Gupta, M. F. Prodanov, W. Zhang, V. V. Vashchenko, T. Dudka, A. L. Rogach, A. K. Srivastava, *Nanoscale* **2019**, *11*, 20837.
 [25] M. Mohammadimasoudi, Z. Hens, K. K. Neyts, *RSC Adv.* **2016**, *6*, 55736.
 [26] Z. Hens, I. Moreels, *J. Mater. Chem.* **2012**, *21*, 10406.
 [27] Y. Y. Ussembayev, Z. Hens, K. Neyts, *ACS Photon.* **2019**, *6*, 1146.
 [28] J. Planelles, F. Rajadell, J. I. Climente, *J. Phys. Chem. C* **2016**, *48*, 27724.
 [29] L. Carbone, C. Nobile, M. De Giorgi, F. D. Sala, G. Morello, P. Pompa, M. Hytch, E. Snoeck, A. Fiore, I. R. Franchini, M. Nadasan, A. F. Silvestre, L. Chiodo, S. Kudera, R. Cingolani, R. Krahne, L. Manna, *Nano Lett.* **2007**, *7*, 2942.
 [30] I. Coropceanu, A. Rossinelli, J. R. Caram, F. S. Freyria, M. G. Bawendi, *ACS Nano* **2016**, *10*, 3295.
 [31] C. Pu, J. Ma, H. Qin, M. Yan, T. Fu, Y. Niu, X. Yang, Y. Huang, F. Zhao, X. Peng, *ACS Central Sci.* **2015**, *2*, 32.
 [32] D. A. Hanifi, N. D. Bronstein, B. A. Koscher, Z. Nett, J. K. Swabeck, K. Takano, A. M. Schwartzberg, L. Maserati, K. Vandewal, Y. van de Burgt, A. Salleo, A. P. Alivisatos, *Science* **2019**, *363*, 1199.
 [33] D. J. Farrell, A. J. Chatten, Pvtrace: Release to Enable DOI Integration, **2014**, <https://doi.org/10.5281/zenodo.12820>.
 [34] P. Moraitis, R. E. I. Schropp, W. van Sark, *Opt. Mater.* **2018**, *84*, 636.